





# Disulfiram blocks inflammatory TLR4 signaling by targeting MD-2

Yang Bai<sup>a,b,1</sup>, Rui Min<sup>a,b,1</sup>, Pengcheng Chen<sup>a,1</sup>, Shenglin Mei<sup>c</sup>, Fan Deng<sup>a,b</sup>, Zengzhang Zheng<sup>a,d</sup>, Cong Jiang<sup>e</sup>, Rui Miao<sup>f,g</sup>, Zeyu Wu<sup>a,b</sup>, Peng Zhang<sup>e</sup>, Youdong Pan<sup>h,i</sup>, Judy Lieberman<sup>f,g,2</sup> , and Xing Liu<sup>a,d,2</sup> 

Contributed by Judy Lieberman; received April 20, 2023; accepted June 23, 2023; reviewed by Katherine A. Fitzgerald and Nan Yan

Toll-like receptor 4 (TLR4) sensing of lipopolysaccharide (LPS), the most potent pathogen-associated molecular pattern of gram-negative bacteria, activates NF- $\kappa$ B and Irf3, which induces inflammatory cytokines and interferons that trigger an intense inflammatory response, which is critical for host defense but can also cause serious inflammatory pathology, including sepsis. Although TLR4 inhibition is an attractive therapeutic approach for suppressing overexuberant inflammatory signaling, previously identified TLR4 antagonists have not shown any clinical benefit. Here, we identify disulfiram (DSF), an FDA-approved drug for alcoholism, as a specific inhibitor of TLR4-mediated inflammatory signaling. TLR4 cell surface expression, LPS sensing, dimerization and signaling depend on TLR4 binding to MD-2. DSF and other cysteine-reactive drugs, previously shown to block LPS-triggered inflammatory cell death (pyroptosis), inhibit TLR4 signaling by covalently modifying Cys133 of MD-2, a key conserved residue that mediates TLR4 sensing and signaling. DSF blocks LPS-triggered inflammatory cytokine, chemokine, and interferon production by macrophages *in vitro*. In the aggressive N-methyl-4-phenyl-1,2,3,6-tetrahydropyridine mouse model of Parkinson's disease (PD) in which TLR4 plays an important role, DSF markedly suppresses neuroinflammation and dopaminergic neuron loss, and restores motor function. Our findings identify a role for DSF in curbing TLR4-mediated inflammation and suggest that DSF and other drugs that target MD-2 might be useful for treating PD and other diseases in which inflammation contributes importantly to pathogenesis.

DSF | TLR4 | MD-2 | cysteine-reactive covalent inhibitor | Parkinson's disease

Toll-like receptors (TLRs), cell-surface and endosomal pattern recognition receptors (PRRs), initiate inflammatory immune responses by recognizing topologically extracellular “nonself” molecules derived from invading microbes pathogen-associated molecular patterns (PAMPs) or aberrant “self” molecules released from damaged or dying host cells (damage-associated molecular patterns, DAMPs) (1–4). TLR4, the first identified TLR in mammals, senses lipopolysaccharide (LPS), heat shock proteins as well as fatty acids (5–8). TLR4 is a type I transmembrane protein, composed of an extracellular region with leucine-rich repeats (LRRs), a transmembrane region and an intracellular toll/interleukin-1 receptor (TIR) domain. MD-2, an 18-kDa glycoprotein without any transmembrane domain, binds the extracellular LRR domain of TLR4 to form a complex (9, 10). MD-2 is critical for TLR4 folding, cell surface trafficking, ligand recognition, and downstream signaling (9–13). When TLR4 senses a ligand, the TLR4 TIR domain recruits Interleukin-1 receptor-associated kinase 4 (IRAK4), IRAK1, adaptor protein myeloid differentiation factor 88 (MyD88), and tumor necrosis factor receptor-associated factor 6 (TRAF6) to form a complex that activates transforming growth factor  $\beta$ -activated kinase 1 (TAK1). Active TAK1 in turn phosphorylates inhibitor of nuclear factor NF- $\kappa$ B (I $\kappa$ B) kinases  $\alpha$  and  $\beta$  (IKK $\alpha$ / $\beta$ ), which phosphorylate and degrade I $\kappa$ B, releasing nuclear factor (NF)- $\kappa$ B to translocate to the nucleus to initiate the transcription of proinflammatory cytokines (1, 7, 14, 15). Meanwhile TLR4 also induces type I interferons (IFN) by activating the TLR adaptor molecule 1 (TICAM1/TRIF)-TANK-binding kinase 1 (TBK1)-interferon regulatory factor 3 (IRF3) pathway (15).

PAMP- or DAMP-triggered TLR4-mediated immune responses help control infection, tissue repair, and regeneration, while excessive activation of TLR4 causes inflammation associated with the onset and development of inflammatory disorders, including cytokine storm, septic shock, and neurodegenerative diseases (16–20). The pathology of type II diabetes, atherosclerosis, and cerebral ischemia injury is also exacerbated by TLR4-driven inflammation (21–26). Aberrant TLR4 activation has also been implicated in schizophrenia and autism (27, 28). Recent studies found that TLR4-mediated inflammation is involved in the pathogenesis of Parkinson's disease (PD), a neurodegenerative disease that

## Significance

In response to pathogen/damage-associated molecular patterns, Toll-like receptor 4 (TLR4) initiates a host innate immune inflammatory response to control infection, tissue repair, and regeneration, while aberrant activation of TLR4 causes tissue damage and various inflammatory diseases. Therefore, TLR4 signaling is an attractive drug target for the treatment of TLR4-driven inflammatory disorders. Here, we showed that the FDA-approved drug disulfiram inhibits TLR4 signaling in both human and mouse cells by modifying a cysteine residue of MD-2, a critical cofactor of TLR4, and found that DSF markedly ameliorates TLR4-mediated pathology in an aggressive mouse model of Parkinson's disease (PD). This study suggests an approach to treating TLR4-mediated inflammatory diseases.

Author contributions: Y.B., R. Min, P.C., J.L., and X.L. designed research; Y.B., R. Min, P.C., F.D., Z.Z., C.J., R. Miao, and Z.W. performed research; P.Z. and Y.P. contributed new reagents/analytic tools; Y.B., R.M., P.C., S.M., F.D., Z.Z., C.J., J.L., and X.L. analyzed data; and Y.B., R. Min, J.L., and X.L. wrote the paper.

Reviewers: K.A.F., University of Massachusetts Medical School; and N.Y., UT Southwestern Medical Center.

Competing interest statement: J.L., Co-founder and SAB member, Ventus Therapeutics.

Copyright © 2023 the Author(s). Published by PNAS. This article is distributed under [Creative Commons Attribution-NonCommercial-NoDerivatives License 4.0 \(CC BY-NC-ND\)](https://creativecommons.org/licenses/by-nc-nd/4.0/).

<sup>1</sup>Y.B., R. Min, and P.C. contributed equally to this work.

<sup>2</sup>To whom correspondence may be addressed. Email: [judy.lieberman@childrens.harvard.edu](mailto:judy.lieberman@childrens.harvard.edu) or [xingliu@iaps.ac.cn](mailto:xingliu@iaps.ac.cn).

This article contains supporting information online at <https://www.pnas.org/lookup/suppl/doi:10.1073/pnas.2306399120/-DCSupplemental>.

Published July 24, 2023.

destroys dopaminergic neurons in the brain (19, 20). Genetic deficiency of *Tlr4* or its inhibition reduces neuroinflammation and prevents PD in mouse models (29, 30). However, what activates TLR4 in PD is not clear.

In this study, we found that disulfiram (DSF), an FDA-approved drug used to treat alcohol addiction, blocked TLR4 signaling by covalently modifying a key conserved Cys-residue of MD-2, required for activating TLR4. Other Cys-reactive compounds, afatinib and dimethyl fumarate (DMF), also inhibited TLR4 signaling, which depended on their Cys-reactivity. In the 1-methyl-4-phenyl-1,2,3,6-tetrahydropyridine (MPTP) neurotoxin mouse model of PD, DSF markedly suppressed neuroinflammation, dopaminergic neuron dropout, and the functional deficits of PD.

## Results

### DSF Specifically Inhibits LPS-Triggered Inflammatory Response.

Both DSF and Bay 11-7082 potently inhibit gasdermin D (GSDMD) pore formation to block inflammatory cell death (31,

32). Because Bay 11-7082 also antagonizes IKK and thus inhibits NF- $\kappa$ B signaling (33, 34), we assessed whether DSF might also inhibit the NF- $\kappa$ B pathway that primes inflammasome signaling. To examine the effect of DSF on NF- $\kappa$ B activation, we pretreated mouse immortalized bone marrow-derived macrophages (iBMDMs) with DSF and then stimulated them with different NF- $\kappa$ B signaling activators, including tumor necrosis factor  $\alpha$  (TNF $\alpha$ , ligand of tumor necrosis factor receptor), peptidoglycan (PGN, ligand of TLR2), LPS (ligand of TLR4), and flagellin (FLN, ligand of TLR5), and assessed NF- $\kappa$ B transcriptional activation. In the absence of DSF, all of these stimuli potently activated mRNA expression of the NF- $\kappa$ B-dependent genes, *Il1b*, *Il6*, *Il12b*, *Tnfa*, *Ccl2*, *Ccl5*, and *Cxcl10* within 4 h (Fig. 1A and *SI Appendix*, Fig. S1 A–C). Unexpectedly, DSF specifically blocked TLR4-dependent NF- $\kappa$ B-mediated gene expression in response to LPS, but only modestly inhibited *Il1b* expression and either increased or did not significantly change the expression of the other NF- $\kappa$ B-dependent genes tested after TNFR, TLR2, or TLR5 stimulation (Fig. 1A and *SI Appendix*, Fig. S1 A–C). In parallel, DSF blocked TLR4, but not TLR2 or TLR5, stimulation of interferon (*Ifnb*) and the interferon-stimulated

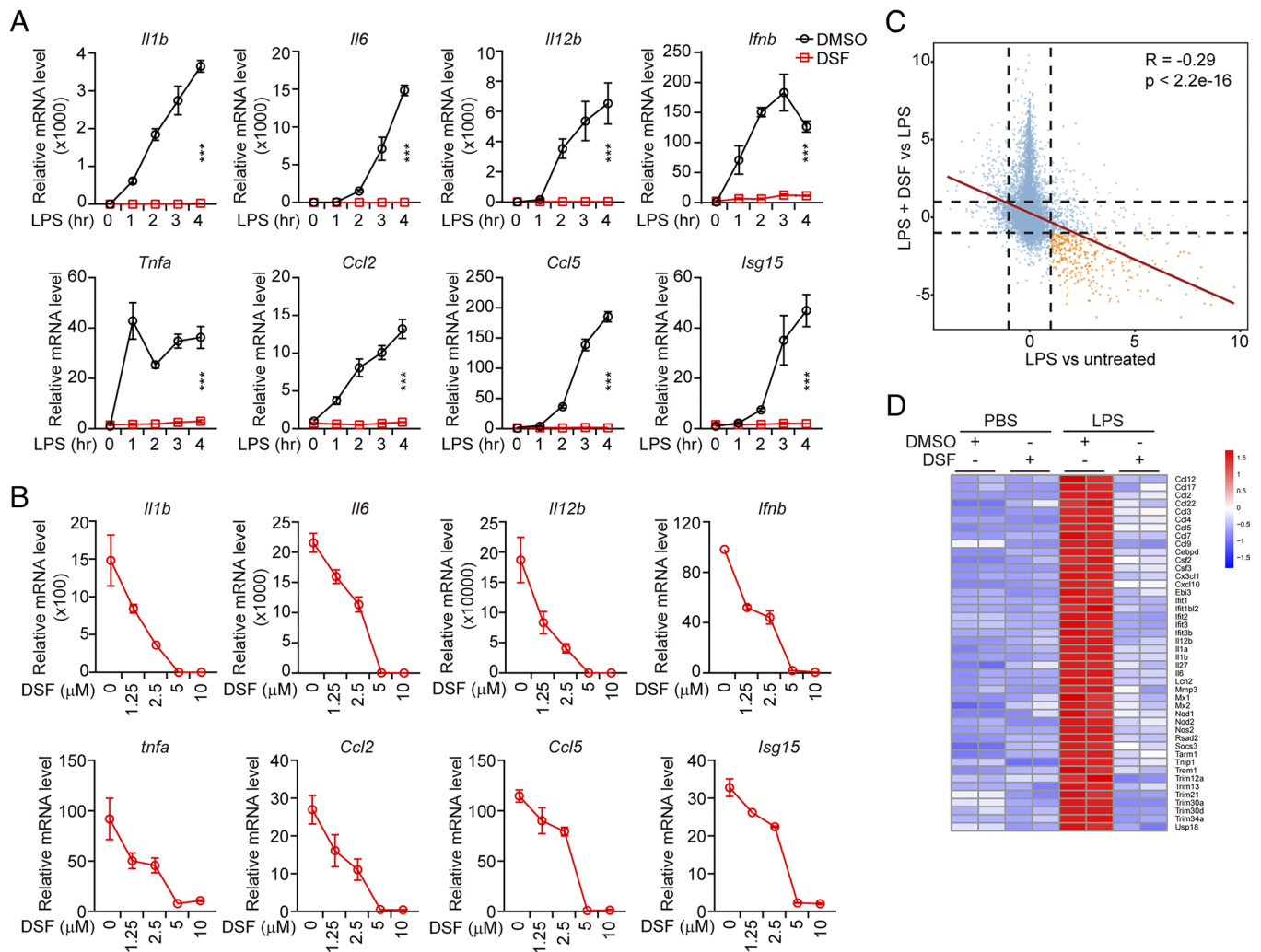


**Fig. 1.** DSF inhibits the LPS-triggered inflammatory response. (A) Mouse iBMDMs were pretreated or not with DSF (5  $\mu$ M) for 0.5 h before stimulation with LPS (1  $\mu$ g/mL) for the indicated times. mRNA levels of the indicated inflammatory cytokines were assessed by qRT-PCR, normalized to *Gapdh* and relative to unstimulated cells. (B) Mouse iBMDMs were pretreated with the indicated concentrations of DSF for 0.5 h before stimulation with LPS (1  $\mu$ g/mL). mRNA levels of the indicated inflammatory cytokines were assessed by qRT-PCR, normalized to *Gapdh* and relative to unstimulated cells. (C and D) RNAseq analysis of RNA expression in mouse iBMDMs treated or not with LPS in the presence or absence of DSF (5  $\mu$ M). (C) Differential gene expression after treatment with LPS in the presence vs. absence of DSF (Y axis) or LPS treatment vs. untreated controls (X axis). The dotted lines represent log (fold change) = 1. (D) Heatmap of genes filtered by adjusted *P* value < 0.05 and the absolute log<sub>2</sub> fold change > 2 after treatment with LPS compared to untreated control. Graphs in A and B show mean  $\pm$  SD; data are representative of three independent experiments. Data were analyzed using two-way ANOVA. \*\*\**P* < 0.001.

gene 15 (*Isg15*) (Fig. 1A, and *SI Appendix, Fig. S1 B and C*). DSF inhibited LPS-mediated induction of both NF- $\kappa$ B and IRF3 regulated genes in a dose-dependent manner – DSF inhibition was detected at the lowest concentration tested (1.25  $\mu$ M), and gene induction was completely blocked at 5 and 10  $\mu$ M (Fig. 1B). DSF was even more active at blocking TLR4 signaling than at blocking canonical and noncanonical inflammasome-induced GSDMD pore formation and pyroptosis, which was previously reported in dose–response experiments to plateau at concentrations >20  $\mu$ M in the same cells (31). To confirm the effectiveness of DSF to inhibit LPS activation of TLR4 signaling, triplicate libraries prepared from iBMDMs that were pretreated or not with DSF and then challenged or not with LPS were analyzed by RNA-seq (35). LPS-triggered induction and inhibition of downstream genes was blocked in the presence of DSF (Fig. 1C). The genes up-regulated in response to LPS, whose induction was blocked by DSF, were proinflammatory genes known to be induced by TLR4 activation (Fig. 1D). The inhibitory effect of DSF on TLR4 signaling was also confirmed in human monocyte-like THP-1 cells (*SI Appendix, Fig. S1D*). These data suggest that DSF potently inhibits TLR4 signaling in both human and mouse cells.

**Copper Improves DSF Inhibition of TLR4 Signaling.** In vivo DSF undergoes rapid metabolic conversion by glutathione to diethyldithiocarbamate (DTC), which chelates with copper (Cu(II))

to form a DTC–copper complex (CuL<sub>2</sub>) (36, 37) (Fig. 2A). Because the bioactivity of DSF is markedly improved by Cu(II), we examined whether Cu(II) also enhances DSF inhibition of TLR4 signaling by measuring half-maximal inhibitory concentration (IC<sub>50</sub>) values of DSF in LPS-treated iBMDMs (Fig. 2B). The cellular IC<sub>50</sub>s of DSF for inhibiting LPS induction of *Il1b*, *Il6*, and *Il12b* in the absence of Cu(II) were 2.74  $\pm$  0.46  $\mu$ M, 2.03  $\pm$  0.29  $\mu$ M, and 1.91  $\pm$  0.60  $\mu$ M, respectively, which was lower than the reported IC<sub>50</sub> (~10  $\mu$ M) of DSF for blocking GSDMD-mediated pyroptosis (31). In the presence of Cu(II), the IC<sub>50</sub> of DSF for blocking LPS induction of *Il1b*, *Il6*, and *Il12b* decreased 3-fold to 11-fold to 0.24  $\pm$  0.05  $\mu$ M, 0.28  $\pm$  0.02  $\mu$ M, and 0.35  $\pm$  0.11  $\mu$ M, respectively (Fig. 2B). Addition of Mg(II) in place of Cu(II) had little effect on DSF activity (Fig. 2C). Neither Cu(II) nor Mg(II) on its own inhibited TLR4 signaling (*SI Appendix, Fig. S2*). Thus, copper improves the potency of DSF inhibition of TLR4 inflammatory signaling.

**DSF Inhibition of TLR4 Signaling Is Independent of GSDMD and Caspase-1.** Because DSF directly targets GSDMD and blocks its pore-forming activity in cells and also inhibits GSDMD and the inflammatory caspases in vitro, we assessed whether the inhibitory effect of DSF on TLR4 signaling was caused by the blockade of the inflammasome–GSDMD pathway by DSF. To this end, *Gsdmd*- or *caspase-1*-deficient iBMDMs, generated using CRISPR-based gene editing (*SI Appendix, Fig. S3 A–C*), were stimulated with

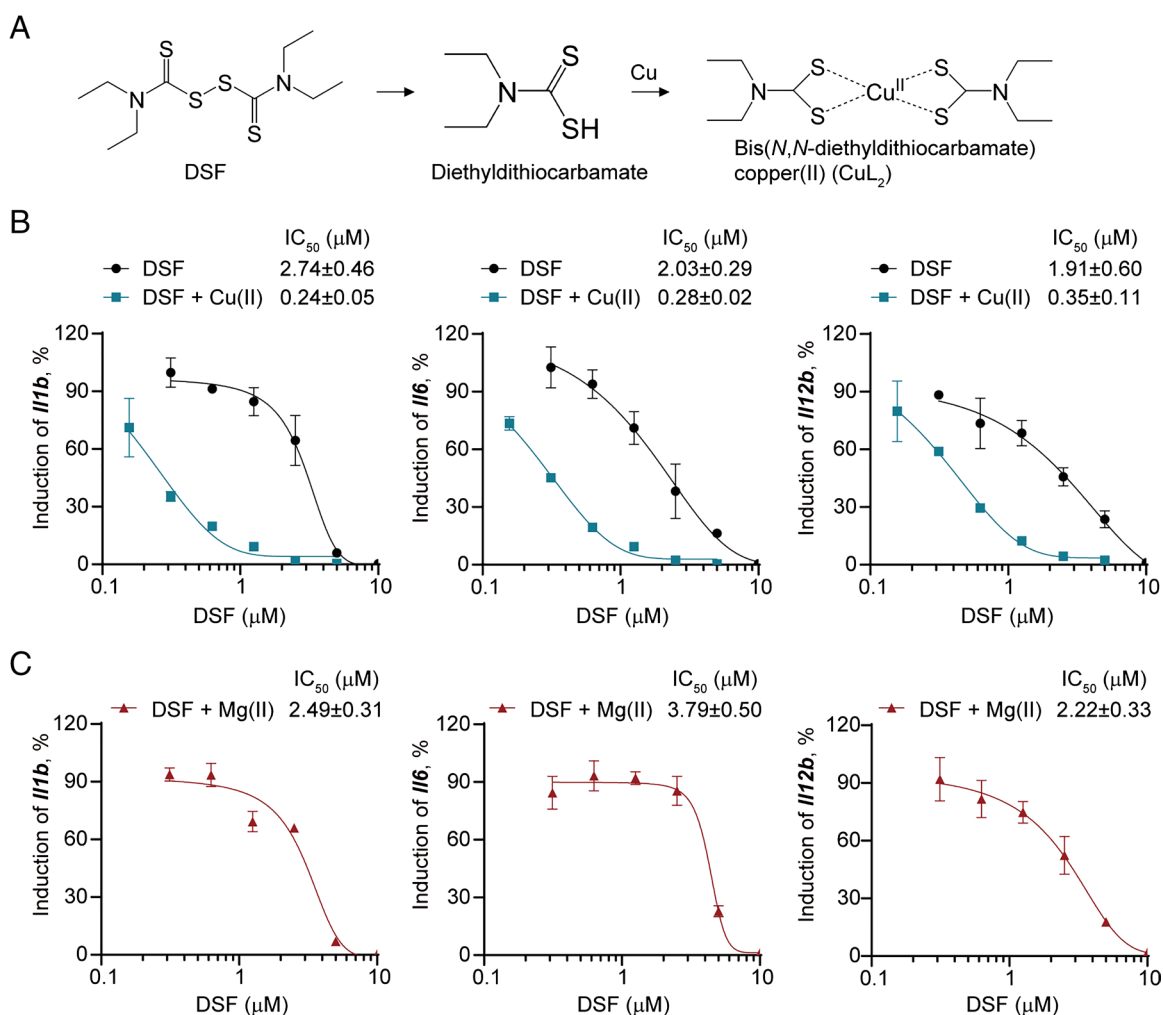


**Fig. 2.** DSF inhibition is markedly enhanced in the presence of Cu(II). (A) DSF is rapidly metabolized to DTC, which forms a complex with Cu(II). (B and C) Dose–response curves of inhibition of TLR4-induced proinflammatory cytokine expression by DSF in the absence or presence of Cu(II) (B) or Mg(II) (C) in iBMDMs. Graphs show mean  $\pm$  SD; data are representative of three independent experiments.



LPS in the presence or absence of DSF. The protein level of key factors in TLR4-mediated NF- $\kappa$ B activation, including Irak4, I $\kappa$ B $\alpha$ , and p65, was unaltered by *Gsdmd* or *Casp1* knockout (SI Appendix, Fig. S3C). In response to LPS treatment, the induction of *Il1b*, *Il6*, and *Il12b* in *Gsdmd*- or caspase-1-deficient iBMDMs was similar to that in wild-type (WT) cells, indicating that neither *Gsdmd* nor caspase-1 is involved in TLR4 signaling (SI Appendix, Fig. S3D). DSF was unimpaired in inhibiting the LPS induction of these inflammatory cytokines in *Gsdmd*- or caspase-1-deficient iBMDMs compared to WT iBMDMs. Thus, DSF blockade of TLR4 signaling does not depend on the inflammasome–GSDMD axis.

To further assess the dual effects of DSF on both TLR4-mediated priming and GSDMD membrane pore formation, we compared WT iBMDMs treated with DSF before and after priming, with *Tlr4*<sup>-/-</sup> and *Gsdmd*<sup>-/-</sup> iBMDMs. Induction of *Il1b* mRNA and mature IL-1 $\beta$  secretion are early-phase (priming) and late-phase (pyroptosis) readouts, respectively. As expected, application of DSF before, but not after LPS treatment, blocked priming (SI Appendix, Fig. S3 E and F). No priming occurred in TLR4-deficient iBMDMs under either condition (SI Appendix, Fig. S3 E and F). In comparison, and as expected, nigericin-triggered IL-1 $\beta$  secretion, which depends on TLR4 for *Il1b* expression and on GSDMD for release, was abrogated in WT iBMDMs by DSF and in both *Gsdmd*-deficient and *Tlr4*-deficient iBMDMs in the absence of DSF (SI Appendix, Fig. S3 G and H). These data highlight the dual roles of DSF in inhibiting both upstream and downstream inflammatory responses.

**TLR4 Sensing of LPS Is the Main Target of DSF.** To elucidate the cellular mechanism of DSF acting on TLR4 signaling, we first

assessed the effect of LPS on NF- $\kappa$ B expression using a luciferase reporter assay with LPS stimulation or exogenous overexpression of signaling molecules involved in TLR4 signaling. Consistent with DSF suppression of NF- $\kappa$ B-induced gene expression (Fig. 1), DSF suppressed LPS activation of the NF- $\kappa$ B-luciferase reporter (Fig. 3A). However, although ectopic overexpression of key TLR4 signaling molecules, including MyD88, TRAF6, TAK1 + TAB1, IKK $\beta$ , and p65, robustly induced the NF- $\kappa$ B-luciferase reporter (Fig. 3 B and C), DSF did not suppress their activation of the NF- $\kappa$ B-luciferase reporter. These results suggest that DSF interferes with LPS sensing by the upstream TLR4 signalosome rather than by inhibiting molecules that mediate downstream signaling. This finding is consistent with the specificity of DSF for TLR4 and not TLR2 or TLR5, which use the same downstream signaling pathway. Next, we examined by immunoblot (Fig. 3D) and immunofluorescence microscopy (Fig. 3E) how DSF affected the key molecular events of TLR4 signaling. LPS triggered the phosphorylation of IKK $\beta$ , I $\kappa$ B $\alpha$ , p65, degradation of I $\kappa$ B $\alpha$ , nuclear translocation of p65, and induced expression of IL-1 $\beta$ , which were all blocked with DSF pretreatment. By contrast, DSF had no effect on TNF $\alpha$ -induced nuclear translocation of p65 (SI Appendix, Fig. S4). These data suggested that TLR4 sensing of LPS is the main step in TLR4 activation that is blocked by DSF.

**DSF Modifies MD-2 on Cys133 to Inhibit TLR4 Activation.** As a thiol-reactive compound, DSF targets and covalently modifies substrate proteins on cysteine residues, which prevents their oxidation. In cells glutathione is the major molecule responsible for reducing oxidized cysteines. Glutathione is depleted during cellular oxidative stress and its levels can be increased by treatment

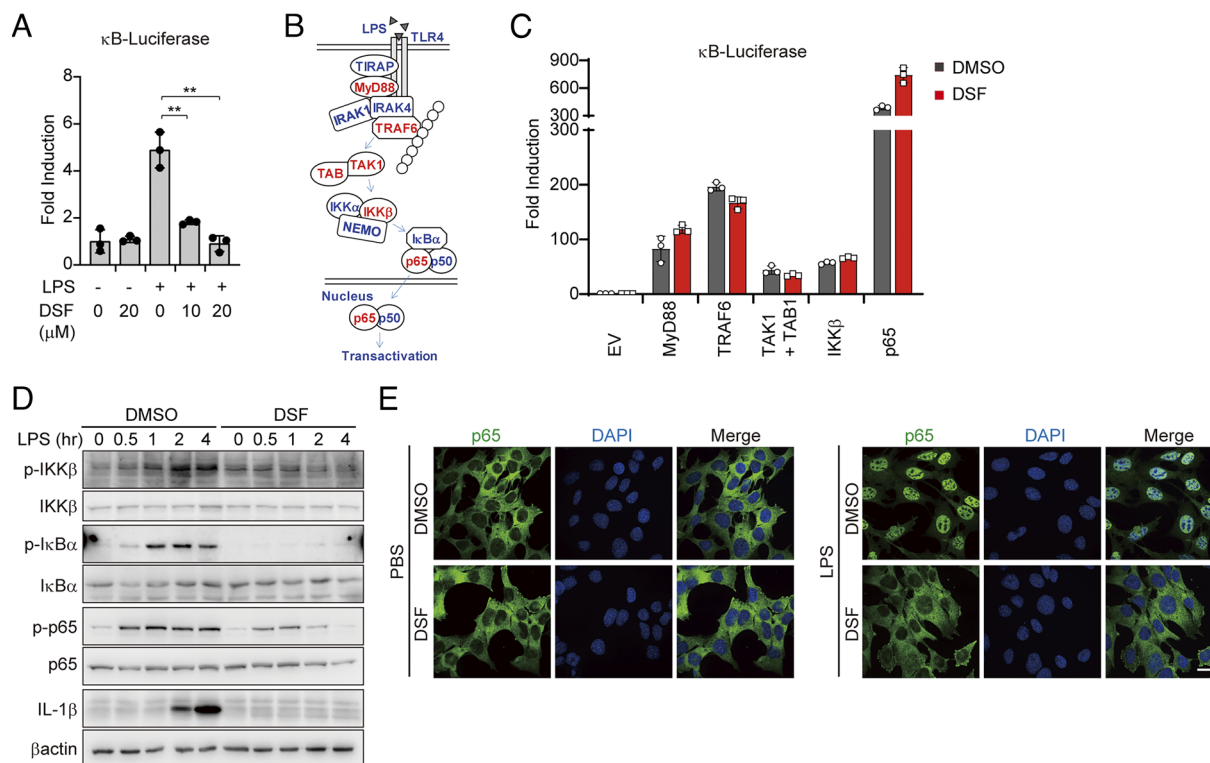


**Fig. 3.** DSF targets the TLR4 signalosome. (A) RAW 264.7 cells transfected with Firefly 5 $\times$  $\kappa$ B-luciferase and pTK-Renilla reporters were pretreated or not with LPS in the absence or presence of DSF and analyzed by dual luciferase reporter assay. (B) Schematic diagram of TLR4 signaling pathway. (C) HEK293T cells, transfected with 5 $\times$  $\kappa$ B-luciferase and pTK-Renilla reporters together with the indicated expression plasmids for 6 h, were treated or not with DSF (20  $\mu$ M) and analyzed by dual luciferase assay 18 h later. (D) iBMDMs, pretreated with DSF (5  $\mu$ M) or DMSO for 0.5 h before stimulation with LPS (1  $\mu$ g/mL), were harvested at the indicated time points for immunoblotting probed for IKK $\beta$ , I $\kappa$ B $\alpha$  and NF- $\kappa$ B p65 phosphorylation and IL-1 $\beta$  induction. (E) MEF cells, pretreated or not with DSF (5  $\mu$ M) for 0.5 h, were stimulated with LPS (1  $\mu$ g/mL) for another 0.5 h, before staining for NF- $\kappa$ B p65. Representative immunofluorescence images of NF- $\kappa$ B p65 subcellular localization are shown. Graphs in A and C show mean  $\pm$  SD; data are representative of three independent experiments. Data were analyzed using a two-tailed Student's *t* test. **\*\****P* < 0.01.

with N-acetyl-L-cysteine (NAC) or antioxidants such as the superoxide scavenger Tiron. To determine whether the inhibitory effect of DSF on TLR4 signaling depends on its thiol-reactivity, iBMDMs were pretreated with Tiron or N-acetyl-L-cysteine (NAC) before they were stimulated with LPS. Both Tiron and NAC markedly reduced DSF inhibition of LPS-mediated proinflammatory cytokine induction (Fig. 4 *A* and *B*), suggesting that thiol-reactivity is required for DSF to inhibit TLR4 signaling. MD-2 is an extracellular glycoprotein that binds to the LRR sensing region of TLR4 and enhances TLR4 ligand binding in a process that depends on a reactive cysteine (Cys133), which is evolutionarily conserved (*SI Appendix, Fig. S5*) (38, 39), suggesting that MD-2 might be the target of DSF. To test this hypothesis and identify any Cys that reacted with DSF, nano-liquid chromatography–tandem mass spectrometry (nano-LC–MS/MS) was performed on recombinant MD-2 treated or not with DSF and then treated with iodoacetamide to stabilize any free cysteines. Tryptic fragments identified covalent attachment of DTC to MD-2 Cys133 (Fig. 4*C*). In agreement with these observations, DSF abrogated the cell internalization of LPS with TLR4 and MD-2, but had no effect on the expression of cell surface TLR4/MD-2 complex (Fig. 4 *D* and *E*), which is consistent with previous findings that MD-2

Cys133 is critical for the TLR4/MD-2 complex to bind and be activated by LPS (39, 40). Addition of untreated recombinant MD-2 to the medium of iBMDMs pretreated with DSF partially rescued LPS-stimulated inflammatory cytokine gene expression (Fig. 4*F*). Thus, DSF inhibits TLR4 sensing by modifying Cys133 on MD-2.

#### Other Cysteine-Reactive Compounds Inhibit TLR4 Signaling.

To determine whether cysteine modification is a more general mechanism to inhibit TLR4 signaling, we tested the effects on TLR4 signaling of two other cysteine-reactive compounds, afatinib and DMF. Like DSF, both afatinib and DMF significantly down-regulated LPS-triggered induction of *Il1b*, *Il6*, and *Il12b* in a dose-dependent manner (Fig. 5 *A* and *B*). However, afatinib and DMF inhibited TLR4 signaling less than DSF (Fig. 5 *A* and *B*). Both afatinib and DMF inhibited LPS-triggered phosphorylation of IκBα and p65 and induction of IL-1β, IL-6, and TNFα protein (Fig. 5 *C* and *D* and *SI Appendix, Fig. S6*). TLR4 inhibition by afatinib and DMF was mediated by their cysteine-reactivity because NAC reduced their inhibitory effects on inflammatory cytokine expression (Fig. 5 *E* and *F*). Collectively, these data highlight the critical role of protein cysteines in TLR4 signaling

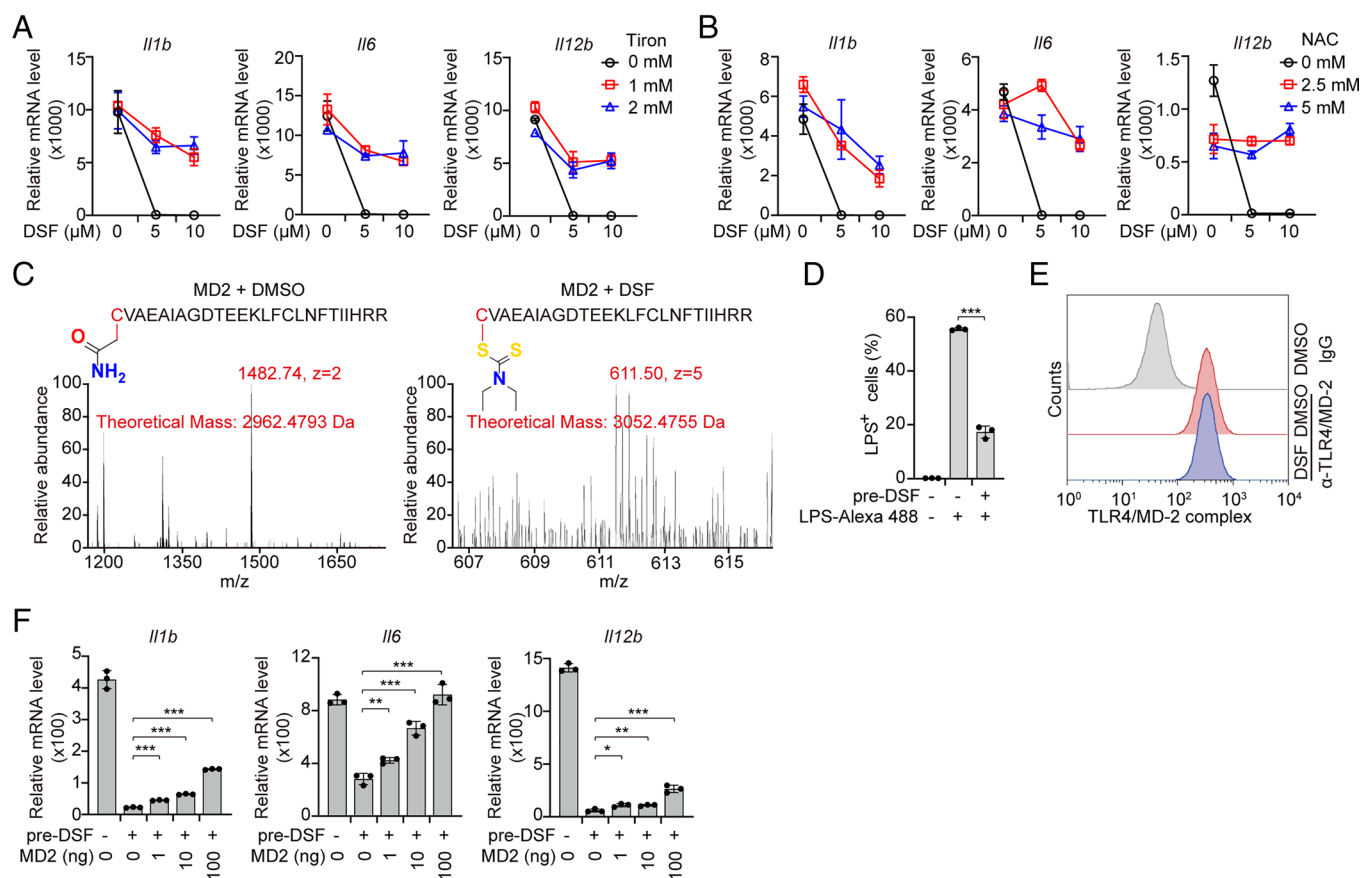


**Fig. 4.** DSF modifies Cys133 of MD-2. (*A* and *B*) iBMDMs were pretreated with the indicated doses of DSF in the presence or absence of Tiron (*A*) or N-acetyl-L-cysteine (NAC) (*B*) for 0.5 h before stimulation or not with LPS (1 μg/mL) for 4 h. mRNA levels of the indicated inflammatory cytokines were assessed by qRT-PCR, normalized to *Gapdh* and relative to unstimulated cells. (*A*) *Il1b*, Tiron 1 mM vs. 0 mM  $P = 0.0005$ , 2 mM vs. 0 mM  $P = 0.0029$ ; *Il6*, Tiron 1 mM vs. 0 mM  $P = 0.0012$ , 2 mM vs. 0 mM  $P < 0.0001$ , *Il12b*, Tiron 1 mM vs. 0 mM  $P < 0.0001$ , 2 mM vs. 0 mM  $P < 0.0001$ ; (*B*) *Il1b*, NAC 1 mM vs. 0 mM  $P = 0.0105$ , 2 mM vs. 0 mM  $P = 0.0012$ ; *Il6*, NAC 1 mM vs. 0 mM  $P < 0.0001$ , 2 mM vs. 0 mM  $P < 0.0001$ , *Il12b*, NAC 1 mM vs. 0 mM  $P < 0.001$ , 2 mM vs. 0 mM  $P < 0.0001$ . (*C*) Recombinant mouse MD-2 protein was incubated with DSF or DMSO for 1 h before mass spectrometry analysis. Cys133 on MD-2 modification by DSF is highlighted. The mass-to-charge ratio ( $m/z$ ), nuclear charge ( $z$ ), and theoretical masses of indicated peptides are shown in red. The spectra at the bottom plot relative abundance vs.  $m/z$  ratio. (*D*) Quantitative analysis of internalization of Alexa Fluor™ 488-labeled LPS by iBMDMs pretreated or not with DSF using flow cytometry. (*E*) Representative flow cytometry histograms showing TLR4/MD-2 complex expression on the surface of iBMDM cells treated or not with DSF. (*F*) iBMDMs, pretreated with DSF for 0.5 h and extensively washed to remove DSF, were treated with increasing concentrations of recombinant MD-2 and stimulated with LPS for 4 h before measuring inflammatory cytokine mRNA levels by qRT-PCR. mRNA level was normalized to *Gapdh* and relative to unstimulated cells. Graphs in *A*, *B*, and *F* show mean  $\pm$  SD; data are representative of three independent experiments. Data were analyzed using two-way ANOVA (*A* and *B*) or a two-tailed Student's *t* test (*F*). \* $P < 0.05$ ; \*\* $P < 0.01$ ; \*\*\* $P < 0.001$ .

and show that other cysteine-reactive compounds also inhibit TLR4 sensing of LPS.

**DSF Protects Mice in an Aggressive PD Model.** TLR4 has been suggested to play a major role in PD pathogenesis, since *Tlr4*<sup>-/-</sup> mice are partially protected in the MPTP-induced mouse model of PD (19, 29, 30). *Tlr4*<sup>-/-</sup> mice show less aggregated  $\alpha$ -synuclein, reduced neuroinflammation, including less NF- $\kappa$ B activation, and less neuronal cell death in the substantia nigra (SN) and a reduction in motor deficits. TLR4's role in PD pathogenesis has been presumed to be activation of TLR4 signaling in microglia and other infiltrating myeloid cells, which highly express TLR4, but this has not been demonstrated. It is worth noting that TLR4 is up-regulated in the SN of MPTP-treated mice and that this region of the brain also has reduced glutathione levels, factors that may contribute to the high sensitivity of this brain region. Thus, to probe the *in vivo* effect of DSF on TLR4 signaling and inflammatory pathology, mice challenged with MPTP were administered DSF intraperitoneally around the time of challenge (Fig. 6A). Without DSF, MPTP challenge resulted in marked loss of tyrosine hydroxylase (TH)-positive dopaminergic neurons in the striatum and SN, but DSF on its own did not cause any overt toxicity, consistent with previous studies (Fig. 6B–F) (41–43). DSF treatment dramatically rescued loss of dopaminergic neurons in MPTP-challenged mice and the functional motor deficits in this model, as measured by the turnaround time and total time to

descend in the pole test (Fig. 6B–H). Thus DSF alleviates TLR4-mediated pathogenesis in an aggressive PD model.

## Discussion

This study identified DSF as a potent and selective inhibitor of TLR4-mediated inflammatory signaling. DSF acted by modifying a Cys residue (Cys133) in the TLR-binding partner MD-2, which blocked LPS sensing. We previously showed that DSF also inactivates GSDMD pore formation by binding to a critical Cys residue needed for pore assembly (31). Thus, the innate immune responses to both extracellular LPS and intracellular LPS, generated by intracellular bacterial pathogens or by uptake of outer membrane vesicles produced by gram-negative bacteria, are strongly inhibited by DSF. Moreover, in this study we also showed dramatic protection in a TLR4-dependent and LPS-independent mouse model of PD.

DSF and other Cys-reactive compounds have shown promise for treating both infection-induced and sterile inflammation-related disorders, including sepsis and autoimmune inflammation in mouse models (31, 44–46). In fact, inflammatory pathways are exquisitely sensitive to cellular redox status (20, 47–49). Inflammatory immune pathways are fine-tuned through active cysteines by reactive oxygen species and unpaired Cys's can act as sensors of cellular redox status. Many key inflammatory mediators or regulators, including STING, NLRP3, the inflammatory caspases,

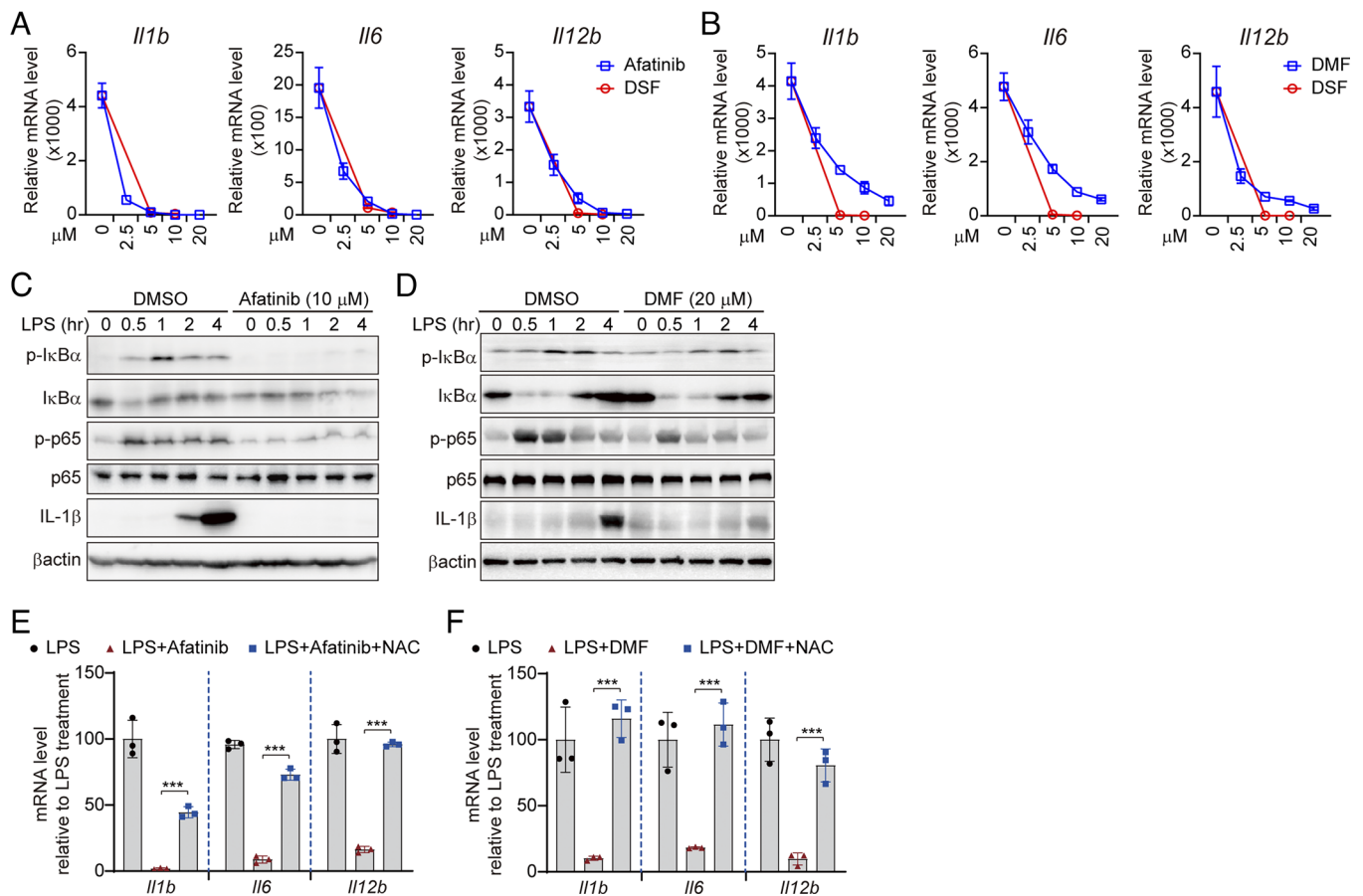


**Fig. 5.** Other cysteine-reactive compounds, afatinib and DMF, inhibit TLR4 signaling. (A and B) iBMDMs were pretreated with afatinib, DMF, or DSF for 0.5 h before stimulation with LPS (1  $\mu$ g/mL) for 4 h. mRNA levels of the indicated inflammatory cytokines were assessed by qRT-PCR, normalized to *Gapdh* and relative to unstimulated cells. (C and D) iBMDMs were pretreated or not with afatinib (10  $\mu$ M) (C) or DMF (20  $\mu$ M) (D) for 0.5 h before stimulation with LPS (1  $\mu$ g/mL). Whole-cell lysates were harvested at the indicated time points for immunoblot analysis. (E and F) iBMDMs, pretreated with afatinib (10  $\mu$ M) or DMF (20  $\mu$ M) in the presence or absence of NAC for 0.5 h, were stimulated with LPS (1  $\mu$ g/mL). mRNA levels of the indicated inflammatory cytokines were assessed by qRT-PCR, normalized to *Gapdh*. Graphs in A, B, E, and F show mean  $\pm$  SD; data are representative of three independent experiments. Data were analyzed using a two-tailed Student's *t* test. \*\*\**P* < 0.001.



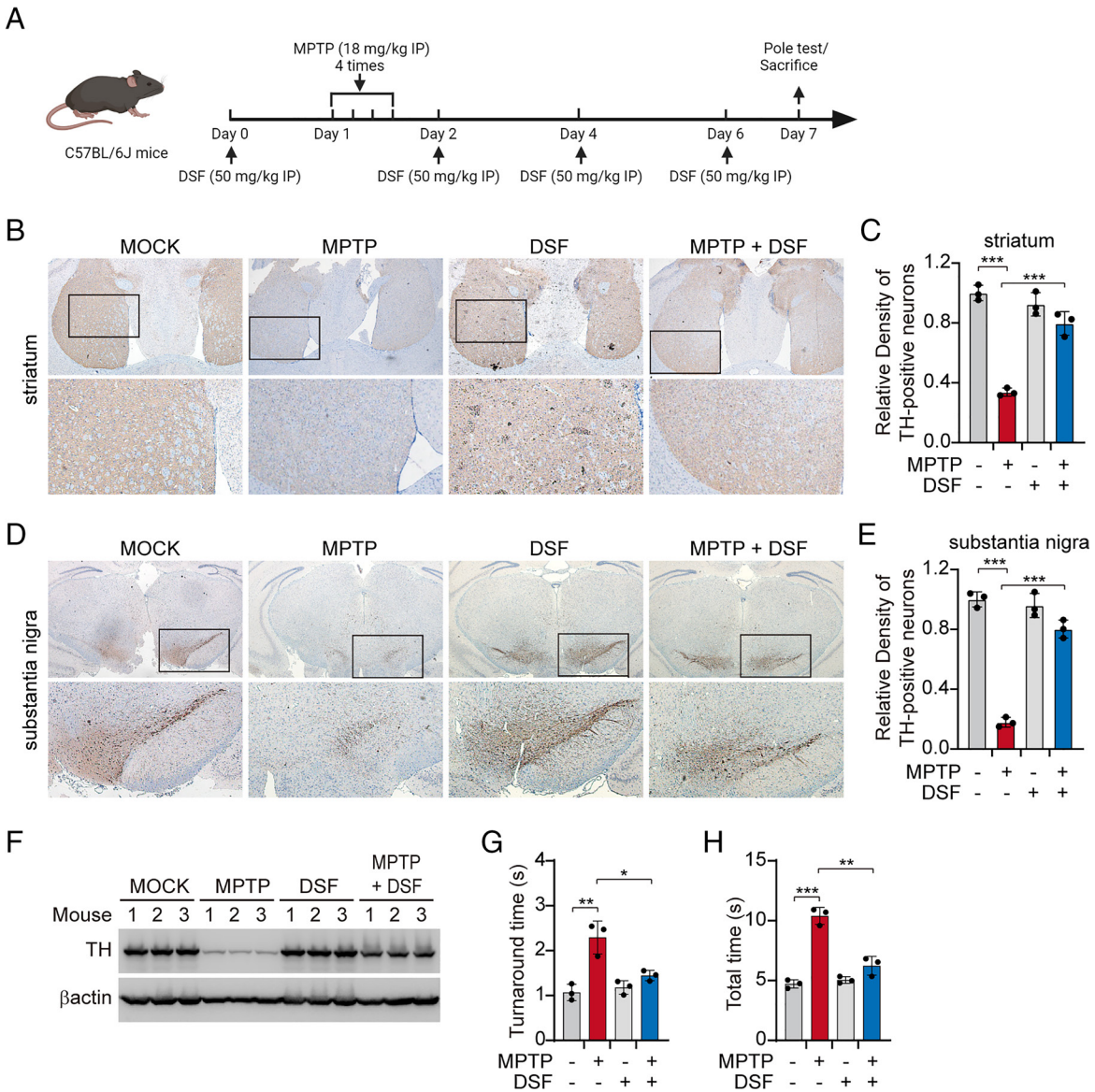


**Fig. 6.** DSF alleviates MPTP-induced PD. (A–H) Mice ( $n = 3$  mice/gp) were injected intraperitoneally with DSF or vehicle 24 h before and every other day after intraperitoneal challenge with MPTP hydrochloride, followed by histopathological (B–E) and immunoblot (F) analysis of tyrosine hydroxylase (TH) in striatum and substantia nigra biopsies from mice brain tissues or motor ability test (G and H) on day 7. Quantification of TH-positive neurons was performed by optical density measurement using ImageJ software (C and E). Graphs in C, E, G, and H show mean  $\pm$  SD; data are representative of three independent experiments. Data were analyzed using a two-tailed Student's *t* test. \* $P < 0.05$ ; \*\* $P < 0.01$ ; \*\*\* $P < 0.001$ .

GSDMD, IKK, and MD-2, have unbound reactive cysteines and compounds that inhibit inflammation (H-151, DSF, DMF, MCC950, Bay11-7082, VX-765) frequently are Cys-reactive. Cys-reactive compounds are notoriously nonspecific in their targets, although the targets that they modify that are critical for their therapeutic benefit can often be identified (i.e., alcohol dehydrogenase for DSF's use in alcoholism or as here TLR4 and GSDMD for preventing LPS toxicity). Although drug developers are reluctant to develop Cys-reactive drugs because of their lack of specificity, the approved Cys-reactive drugs such as DSF and DMF (used for multiple sclerosis) are remarkably well tolerated. The prominence of reactive Cys's in innate immune protein mediators suggests that it is worth seriously considering Cys-reactive compounds for suppressing inflammation in many settings including autoimmune and autoinflammatory diseases.

DSF and DMF were both previously shown to protect mice from LPS-induced sepsis (31, 50, 51). DSF not only protected mice from pyroptotic death, but also strongly inhibited serum

levels of the inflammatory cytokines IL-1 $\beta$ , IL-6, and TNF $\alpha$ , cytokines whose expression is up-regulated by NF- $\kappa$ B. Extracellular LPS is sensed by TLR4, but intracellular LPS is sensed by the cytosolic noncanonical inflammasome (caspase-4 and -5 in humans and caspase-11 in mice), which when activated cleaves GSDMD to cause pyroptosis. Noncanonical inflammasome activation of pyroptosis dominates the pathology of LPS-mediated sepsis in mice since genetic deficiency of either *Gsdmd* or *Casp11* protects mice from lethality (31). Protection from LPS-induced sepsis by DSF and DMF depended on their ability to inhibit cleaved GSDMD pore formation. However, the effectiveness of these drugs in sepsis likely depends on inhibiting both LPS sensing by TLR4 and GSDMD pores.

Similarly, although neither GSDMD nor caspase-1 deficiency affected DSF inhibition of inflammatory cytokine expression in response to LPS in vitro (SI Appendix, Fig. S3D), inhibiting NLRP3 and/or GSDMD pores may contribute to the strong protection provided by these drugs in the in vivo PD model reported

here. In fact, NLRP3, caspase-1, and IL-1 $\beta$  are all activated in the MPTP model of PD and reduced in *Thr4<sup>-/-</sup>* mice (19, 20). Pyroptosis could be a feature of neuronal or microglial cell death in PD. Future studies to examine inflammatory pathways in PD and whether microglia, which express TLR4 and GSDMD, and/or neurons, which highly express GSDME, are undergoing pyroptosis, and their relative contributions to inflammatory pathology will be important for developing strategies to reduce inflammation as an approach to treating PD. It will also be important to understand what the TLR4/MD-2 complex senses in this PD model and whether TLR4/MD-2 plays a pathogenic role in human PD.

## Materials and Methods

**Plasmids and Reagents.** psPAX2, pMD2.G and lentiCRISPR v2 constructs were obtained from Addgene. 5 $\times$  $\kappa$ B-luciferase, Renilla, MyD88, TRAF6, TAK1, TAB1, IKK $\beta$ , NF- $\kappa$ B p65 plasmids were gifts of Professor Chen Wang (China Pharmaceutical University). cDNAs encoding mouse MD-2 were amplified by PCR from the mouse cDNA library, and subcloned into pET-28a, pCDNA3, or pFLAG-CMV4 vectors. All plasmids were verified by sequencing before use. Dimethyl sulfoxide (DMSO),  $\beta$ -mercaptoethanol (2-ME), dithiothreitol (DTT), DSF, afatinib, DMF, copper sulfate, magnesium chloride, Tiron, N-acetyl cysteine (NAC), DAPI, MPTP, LPS, and gentamicin sulfate were purchased from Sigma Aldrich. PGN, flagellin, puromycin, and blasticidin were from Invivogen. Recombinant TNF $\alpha$  was from Peprotech. Recombinant active MD-2 protein (ab238343) purified from 293T cells was from Abcam. The complete protease inhibitor cocktail tablets and the PhosSTOP phosphatase inhibitor cocktail tablets were from Roche. Polyclonal phospho-I $\kappa$ B $\alpha$  (Ser32) (14D4) antibody (#2859), monoclonal I $\kappa$ B $\alpha$  (L35A5) antibody (#4814), monoclonal phospho-NF- $\kappa$ B p65 (Ser536) (7F1) antibody (#3036), monoclonal NF- $\kappa$ B p65 (D14E12) antibody (#8242), polyclonal IRAK4 antibody (#4363), IKK $\beta$  (L570) antibody (#2678), monoclonal Phospho-IKK $\alpha$ / $\beta$  (Ser176/180) (16A6) antibody (#2697), and monoclonal cleaved Caspase-1 (Asp297) (D57A2) antibody (#4199) were from Cell Signaling Technology (CST). Monoclonal  $\beta$ -actin antibody (A1978) was from Sigma Aldrich. Monoclonal GSDMD antibody (ab209845) and monoclonal anti-tyrosine hydroxylase (TH) antibody (ab137869) were from Abcam. Polyclonal IL-1 $\beta$  antibody (AF-401-NA) was from R&D Systems. PE Rat IgG2a,  $\kappa$  isotype Ctrl Antibody (400507) and monoclonal PE rat anti-mouse TLR4 (CD284)/MD-2 Complex Antibody (117605) was from BioLegend. Polyclonal donkey anti-mouse (715-035-151), anti-rabbit (711-035-152), and anti-goat (705-035-003) antibodies conjugated with horseradish peroxidase were from Jackson ImmunoResearch. Alexa Fluor 488 was from Invitrogen.

**Cell Culture and Treatment.** Human HEK293T and HeLa, mouse iBMDMs, RAW 264.7, and MEF were grown in DMEM (Gibco) supplemented with 10% fetal bovine serum (Gibco), 2 mM L-glutamine (Gibco), 50 U/mL penicillin, 50 mg/mL streptomycin (Gibco), and 50  $\mu$ M 2-ME. Human THP-1 cells were grown in Roswell Park Memorial Institute (RPMI) medium 1640 (Gibco) with the same supplements. All cells were regularly checked to be free of mycoplasma contamination. Transient transfection of HEK293T cells and RAW 264.7 cells was performed with Lipofectamine 3000 (Invitrogen) according to the manufacturer's instructions. For induction of proinflammatory cytokine expression, iBMDMs were treated with PGN (TLR2 agonist), LPS (TLR4 agonist), Flagellin (TLR5 agonist), or TNF $\alpha$  (TNFR ligand) for indicated time.

**Real-Time PCR (qRT-PCR) Analysis.** RNA was extracted with TRIzol Reagent (Thermo Fisher Scientific, 15596026) according to the manufacturer's instructions as described. For real-time PCR analysis, cDNA was synthesized with reverse-transcript kit PrimeScript<sup>TM</sup> RT Master Mix (Takara, RR036A). Real-time quantitative PCR was performed using Power SYBRGreen PCR Master Mix (Applied Biosystems, 1711564) on an ABI QuantStudio<sup>TM</sup> 7 Flex instrument. Primers used for detecting specific genes were as follows, *Il1b*-s: 5'-GCA ACT GTT CCT GAA CTC AACT-3', *Il1b*-as: 5'-ATC TTT TGG GGT CCG TCA ACT-3'; *Il-6*-s: 5'-GAG AGG AGA CTT CAC AGA GGA TAC-3', *Il-6*-as: 5'-GTA CTC CAG AAG ACC AGA GG-3'; *Il-12 p40*-s: 5'-TGG TTT GCC ATC GTT TTG CTG-3', *Il-12 p40*-as: 5'-ACA GGT GAG GTT CAC TGT TTCT-3'; *Irfn*-s: 5'-CTT CTC CAC CAC AGC CCT CTC-3', *Irfn*-as: 5'-CCC ACG TCA ATC TTT CCT CTT-3'; *Tnfa*-s: 5'-CCC TCA CAC TCA GAT CAT CTT CT-3', *Tnfa*-as: 5'-GCT ACG ACG TGG GCT ACA G-3'; *Ccl2*-s: 5'-TTA AAA ACC TGG ATC GGA ACC AA-3', *Ccl2*-as:

5'-GCATTA GCTTCA GATTAC CGG GT-3'; *Ccl5*-s: 5'-GCT GCTTTG CCT ACC TCT CC-3', *Ccl5*-as: 5'-TCG AGT GAC AAA CAC GAC TGC-3'; *Isg15*-s: 5'-CAC AGT GAT GCT AGT GGT AC-3', *Isg15*-as: 5'-CTT AAG CGT GTC TAC AGT CTG-3'; *Cxcl10*-s: 5'-CCA AGT GCT GCC GTC ATT TTC-3', *Cxcl10*-as: 5'-GGC TCG CAG GGATGATTT CAA-3'; *Gapdh*-s: 5'-GAA GGG CTC ATG ACCACA GT-3', *Gapdh*-as: 5'-GGATGCAGG GAT GAT GTT CT-3'; *Il1B*-s: 5'-CCA CAG ACC TTC CAG GAG AAT G-3', *Il1B*-as: 5'-GTG CAG TTC AGT GAT CGT ACA GG-3'; *Il6*-s: 5'-CCT GAA CCT TCC AAA GAT GGC-3', *Il6*-as: 5'-TTC ACC AGG CAA GTC TCC TCA-3'; *IFNB*-s: 5'-ATG ACC AAC AAG TGT CTC CTC C-3', *IFNB*-as: 5'-GGA ATC CAA GCA AGT TG TAG CTC-3'; *GAPDH*-s: 5'-CGG AGT CAA CGG ATT TGG TC-3', *GAPDH*-as: 5'-GAC AAG CTT CCC GTT CTC AG-3'.

**RNA-seq Preparation and Analysis.** Biological triplicate RNA-seq libraries were prepared using the VAHTS mRNA-seq V3 library prep kit (Illumina) and sequenced on an Illumina Novaseq 6000 platform (Illumina). Image analysis and base calling were conducted using the Illumina RTA software. Sequencing reads were aligned to the *Mus musculus* reference genome (GRCm39) obtained from GENCODE. R package DESeq2 was used to analyze differential expression and fold change. The differentially expressed genes were subjected to heat map plotting with R package pheatmap.

**Generation of Knockout Cell Lines by CRISPR-Cas9.** HEK293T cells were transfected with lentivirus-packaging plasmids (PMD2.G/psPAX2) and lentiviral vector (lentiCRISPRV2-puro) carrying Cas9 and gRNAs (*Gsdmd* 5'-AGC ATC CTG GCA TTC CGA G-3'; *Caspase-1* 5'-ATAATG AATACA ACC ACT CG-3') by the calcium phosphate precipitation method as previously described (52). Lentivirus-containing medium was collected 72 h later and filtered with a 0.22- $\mu$ m Stericup filter unit (Millipore) to remove cell debris. iBMDMs were then infected with lentiviruses in the presence of 10  $\mu$ g/mL polybrene when cells reached 50 to 60% confluency. Three days after infection, cells were treated with puromycin (5  $\mu$ g/mL) for stable transfection selection. The surviving cells were further resuspended and diluted to seed as single and isolated cells. Gene editing was verified by genome sequencing and immunoblot analysis.

**Reporter Assay.** Cells seeded in 48-well plates were transfected with the reporter plasmids (5 $\times$  $\kappa$ B-luciferase, pTK-Renilla) together with/without plasmids encoding the key mediators of TLR4 signaling (MyD88, TRAF6, TAK1, TAB1, IKK $\beta$ , or NF- $\kappa$ B p65, 200 ng/well) using Lipofectamine 3000 transfection reagent (Invitrogen). Six hours posttransfection, cells were incubated with fresh medium containing DSF or DMSO for another 18 h, before stimulation or not with LPS. Firefly luciferase activity was measured by Dual-luciferase Reporter Assay System (Promega) using a Synergy H1 plate reader (BioTek) with Gene5 software. Renilla luciferase activity was used to normalize transfection efficiency.

**Immunoblot Analysis.** Cells were washed with phosphate buffered saline (PBS, Gibco) and lysed with lysis buffer (50 mM Tris-HCl pH 7.4, 150 mM NaCl, 1% Triton X100) supplemented with complete Protease inhibitor cocktail (Roche) and PhosSTOP phosphatase inhibitor cocktail (Roche). Then, whole-cell lysate samples were prepared by boiling with 5 $\times$ SDS loading buffer (100 mM Tris-HCl pH 6.8, 4% SDS, 0.2% BPB, 20% glycerol, 2%  $\beta$ -ME), and subjected to SDS-polyacrylamide gel electrophoresis. Proteins were transferred to a polyvinylidene fluoride membrane (Millipore), probed with indicated antibodies and visualized using a chemiluminescence ECL kit (Thermo).

**Immunostaining and Imaging.** Cells seeded on coverslips were fixed with 4% paraformaldehyde for 15 min, permeabilized in 0.2% Triton X-100 for 5 min, and blocked with 5% BSA (Sigma Aldrich) diluted with PBS for 1 h. Then, cells were immunostained with an anti-NF- $\kappa$ B p65 antibody (CST #8242) for 2 h followed by an Alexa Fluor 488-conjugated secondary antibody (Invitrogen) for 1 h. Nuclei were counterstained with DAPI (Sigma Aldrich) for 5 min. Cells were extensively washed with PBS for three times between each step. Slides were then mounted using Aqua-Poly/Mount (Dako). Images were captured using an Olympus SpinSR10 Confocal System with 60X objective and Olympus cellSens Dimension software. All images are representative of three independent experiments.

**Measurement of Cytokine Secretion.** Concentrations of IL-6 and TNF- $\alpha$  in cell culture medium were determined using mouse IL-6 (M6000B) and TNF- $\alpha$  (MTA00B) Quantikine ELISA kits (R&D Systems) according to the manufacturer's instructions.



**Recombinant Protein Purification.** *Escherichia coli* (Rosetta) cells harboring pET28a-6 × His-SUMO-MD-2 were grown in LB broth with 50 µg/mL kanamycin at 37 °C. Overnight cells were diluted with fresh medium in a ratio of 1:100 and grown at 37 °C until the OD<sub>600</sub> reached 0.8. IPTG was then added to cells at a final concentration of 0.2 mM to induce the expression of recombinant MD-2 at 16 °C. Cells were collected and homogenized by ultrasonication in lysis buffer (50 mM Tris-HCl pH 8.0, 150 mM NaCl, 5 mM imidazole and 2 mM β-ME). The clarified lysates obtained after centrifugation were incubated with equilibrated Ni-NTA resin (Qiagen) at 4 °C for 4 h and then extensively washed with wash buffer (50 mM Tris-HCl pH 8.0, 150 mM NaCl, 20 mM imidazole and 2 mM β-ME). Recombinant proteins were eluted with elution buffer (50 mM Tris-HCl pH 8.0, 400 mM NaCl and 500 mM imidazole) and treated with SUMO protease ULP1 (ubiquitin-like-specific protease 1) to remove the 6 × His-SUMO tag, followed by further purification with Superdex 200 (10/300) gel-filtration chromatography and mono-Q ion exchange. Purified recombinant proteins were stored in (50 mM Tris pH 8.0, 150 mM NaCl and 5 mM DTT) at –80 °C for long-term use.

**Liquid Chromatography-Mass Spectrometry (LC-MS) Analysis.** Gel bands containing recombinant MD-2 treated or not with DSF were cut into pieces and washed with 50 mM Tris-HCl (pH 8.0)/acetonitrile (1:1, v/v) solution to destain the gel. The gel slices were incubated with 55 mM iodoacetamide for 60 min at room temperature in the dark, followed by treatment with 100% acetonitrile for 10 min. Trypsin digestion solution (15 ng/µL in 50 mM ammonium bicarbonate) was then added to dried gel pieces overnight at 37 °C for digestion. Tryptic peptides were extracted using extraction solution (5% TFA-50% ACN-45% dH<sub>2</sub>O), acidified with 0.1% formic acid (FA), and subjected to LC-MS analysis using an Easy-nLC1200 High Performance Liquid Chromatography system and Q Exactive™ Hybrid Quadrupole-Orbitrap™ Mass Spectrometer (Thermo Fisher Scientific). Data were analyzed using Byonic and MaxQuant1.6.2.10 software.

**Flow Cytometry.** For membrane TLR4-MD2 complex staining, single-cell suspensions of iBMDMs were incubated with the indicated fluorescent dye-conjugated antibodies [PE-conjugated rat IgG isotype control (RTK2758), PE-conjugated anti-mouse TLR4/MD-2 complex (MTS510)] at 4 °C for 20 min in the dark and then washed three times with FACS buffer (PBS plus 2% FBS), followed by analysis on a BD Celesta cytometer using FlowJo software. For LPS internalization assay, iBMDMs pretreated or not with 20 µM DSF at 37 °C were washed and resuspended in FACS buffer. Single-cell suspensions were incubated with 1 µg/mL Alexa Fluor™ 488-conjugated LPS (Thermo-Fisher L23351) for 2 h at 4 °C and washed three times with FACS buffer, before analysis on a BD Celesta cytometer using FlowJo software.

**Animals.** WT C57BL/6 mice were maintained at the specific pathogen-free facility at Institut Pasteur of Shanghai (IPS) with a 12-h light/12-h dark cycle in a standard ambient environment (20 to 26 °C and 30 to 70% humidity with ad libitum access to food and water). All mouse experiments were conducted in accordance with the national animal research guidelines, using protocols approved by the Institutional Animal Care and Use Committee of IPS.

1. C. A. Janeway Jr., R. Medzhitov, Innate immune recognition. *Annu. Rev. Immunol.* **20**, 197–216 (2002).
2. S. W. Brubaker, K. S. Bonham, I. Zanoni, J. C. Kagan, Innate immune pattern recognition: a cell biological perspective. *Annu. Rev. Immunol.* **33**, 257–290 (2015).
3. N. J. Gay, M. Gangloff, Structure and function of Toll receptors and their ligands. *Annu. Rev. Biochem.* **76**, 141–165 (2007).
4. O. Takeuchi, S. Akira, Pattern recognition receptors and inflammation. *Cell* **140**, 805–820 (2010).
5. R. Medzhitov, P. Preston-Hurlburt, C. A. Janeway Jr., A human homologue of the *Drosophila* Toll protein signals activation of adaptive immunity. *Nature* **388**, 394–397 (1997).
6. A. Poltorak *et al.*, Defective LPS signaling in C3H/HeJ and C57BL/10ScCr mice: mutations in Tlr4 gene. *Science* **282**, 2085–2088 (1998).
7. A. Aderem, R. J. Ulevitch, Toll-like receptors in the induction of the innate immune response. *Nature* **406**, 782–787 (2000).
8. J. Y. Lee *et al.*, Reciprocal modulation of Toll-like receptor-4 signaling pathways involving MyD88 and phosphatidylinositol 3-kinase/AKT by saturated and polyunsaturated fatty acids. *J. Biol. Chem.* **278**, 37041–37051 (2003).
9. T. Fujimoto, S. Yamazaki, A. Eto-Kimura, K. Takeshige, T. Muta, The amino-terminal region of toll-like receptor 4 is essential for binding to MD-2 and receptor translocation to the cell surface. *J. Biol. Chem.* **279**, 47431–47437 (2004).
10. H. M. Kim *et al.*, Crystal structure of the TLR4-MD-2 complex with bound endotoxin antagonist Eritoran. *Cell* **130**, 906–917 (2007).

**Drug Administration and MPTP-Induced Mouse PD Model.** For DSF administration, mice were injected intraperitoneally with DSF formulated in sesame oil at a dose of 50 mg/kg on days 0, 2, 4, and 6. PD was induced in male C57BL/6 mice (8 to 10 wk old) by intraperitoneal injection of MPTP hydrochloride (Sigma) using a dose of 18 mg/kg every 2 h for four times on day 1 (43). All mice were subjected to the pole test and killed to harvest brain tissue on day 7.

**Pole Test.** Mice were placed head up on top of a rough surfaced pole (a bar 50 cm in height, 1 cm in diameter with a ball of 0.3 cm in diameter at the top). The time it took the mouse to completely turn downward was recorded as the turn-around time and the time it took to climb down from the pole was recorded as total time. Before the test, the mice were trained repeatedly until each could climb down from the pole immediately. Records were excluded if the mouse hesitated before climbing.

**Histological Analysis.** Fresh brain tissues were embedded with optimal cutting temperature compound (OCT) (Sakura Tissue-TekH) and snap-frozen in liquid nitrogen. Embedded tissues were equilibrated to –20 °C and sectioned using a microtome. Tissue sections were subjected to immunohistochemistry (IHC) by staining with monoclonal anti-tyrosine hydroxylase (TH) antibody (abcam ab137869) and the 3,3'-diaminobenzidine (DAB) staining kit (Vector sk-4100) and hematoxylin staining according to the manufacturer's instructions before mounting using Aqua-Poly/Mount (Dako). Stained sections were imaged by light microscopy (Olympus BX53) with CellSens software. Densitometric analysis of the TH-positive signal was determined as the percentage of brown staining as measured by Image J software.

**Data, Materials, and Software Availability.** All study data are included in the article and/or *SI Appendix*. RNA-seq data are available in the Gene Expression Omnibus (accession number: [GSE237028](https://www.ncbi.nlm.nih.gov/geo/query/acc.cgi?acc=GSE237028)) (35).

**ACKNOWLEDGMENTS.** This work was supported by National Key R&D Program of China (2020YFA0509600 and 2022YFC2304700), Key Research Program of the Chinese Academy of Sciences (ZDBS-LY-SM008), National Natural Science Foundation of China (31972897 and 32122034), Shanghai Pilot Program for Basic Research-Chinese Academy of Sciences, Shanghai Branch (JCYJ-SHFY-2021-009), Strategic Priority Research Program of Chinese Academy of Sciences (XDB29030300), Shanghai Municipal Science and Technology Major Project (2019SHZDZX02 and HS2021SHZX001), Innovative research team of high-level local universities in Shanghai (SHSMU-ZDCX20211002) (X.L.), National Natural Science Foundation of China (32100716) (P.C.), NIH R01CA240955 and R01AI39914 (J.L.).

Author affiliations: <sup>a</sup>The Center for Microbes, Development and Health, Key Laboratory of Molecular Virology and Immunology, Institut Pasteur of Shanghai, Chinese Academy of Sciences, Shanghai 200031, China; <sup>b</sup>University of Chinese Academy of Sciences, Beijing 100049, China; <sup>c</sup>Department of Biomedical Informatics, Harvard Medical School, Boston, MA 02115; <sup>d</sup>Shanghai Huashen Institute of Microbes and Infections, Shanghai 200052, China; <sup>e</sup>Department of Thoracic Surgery, Shanghai Pulmonary Hospital, School of Medicine, Tongji University, Shanghai 200433, China; <sup>f</sup>Program in Cellular and Molecular Medicine, Boston Children's Hospital, Boston, MA 02115; <sup>g</sup>Department of Pediatrics, Harvard Medical School, Boston, MA 02115; <sup>h</sup>Department of Dermatology, Brigham and Women's Hospital, Boston, MA 02115; and <sup>i</sup>Harvard Skin Disease Research Center, Harvard Medical School, Boston, MA 02115

11. R. Shimazu *et al.*, MD-2, a molecule that confers lipopolysaccharide responsiveness on Toll-like receptor 4. *J. Exp. Med.* **189**, 1777–1782 (1999).
12. Y. Nagai *et al.*, Essential role of MD-2 in LPS responsiveness and TLR4 distribution. *Nat. Immunol.* **3**, 667–672 (2002).
13. S. Saitoh, Chaperones and transport proteins regulate TLR4 trafficking and activation. *Immunobiology* **214**, 594–600 (2009).
14. S. I. Miller, R. K. Ernst, M. W. Bader, LPS, TLR4 and infectious disease diversity. *Nat. Rev. Microbiol.* **3**, 36–46 (2005).
15. L. A. O'Neill, D. Golenbock, A. G. Bowie, The history of Toll-like receptors - redefining innate immunity. *Nat. Rev. Immunol.* **13**, 453–460 (2013).
16. T. Gong, L. Liu, W. Jiang, R. Zhou, DAMP-sensing receptors in sterile inflammation and inflammatory diseases. *Nat. Rev. Immunol.* **20**, 95–112 (2020).
17. J. Zindel, P. Kubas, DAMPs, PAMPs, and LAMPs in immunity and sterile inflammation. *Annu. Rev. Pathol.* **15**, 493–518 (2020).
18. M. T. Heneka, D. T. Golenbock, E. Latz, Innate immunity in Alzheimer's disease. *Nat. Immunol.* **16**, 229–236 (2015).
19. M. T. Heneka, M. P. Kummer, E. Latz, Innate immune activation in neurodegenerative disease. *Nat. Rev. Immunol.* **14**, 463–477 (2014).
20. C. K. Glass, K. Saijo, B. Winner, M. C. Marchetto, F. H. Gage, Mechanisms underlying inflammation in neurodegeneration. *Cell* **140**, 918–934 (2010).

21. M. R. Dasu, S. Devaraj, S. Park, I. Jialal, Increased toll-like receptor (TLR) activation and TLR ligands in recently diagnosed type 2 diabetic subjects. *Diabetes Care* **33**, 861–868 (2010).
22. S. C. Hollestelle *et al.*, Toll-like receptor 4 is involved in outward arterial remodeling. *Circulation* **109**, 393–398 (2004).
23. M. Lin *et al.*, The TLR4 antagonist CRX-526 protects against advanced diabetic nephropathy. *Kidney Int.* **83**, 887–900 (2013).
24. M. Lin *et al.*, Toll-like receptor 4 promotes tubular inflammation in diabetic nephropathy. *J. Am. Soc. Nephrol.* **23**, 86–102 (2012).
25. K. S. Michelsen *et al.*, Lack of Toll-like receptor 4 or myeloid differentiation factor 88 reduces atherosclerosis and alters plaque phenotype in mice deficient in apolipoprotein E. *Proc. Natl. Acad. Sci. U.S.A.* **101**, 10679–10684 (2004).
26. J. Qiu *et al.*, High-mobility group box 1 promotes metalloproteinase-9 upregulation through Toll-like receptor 4 after cerebral ischemia. *Stroke* **41**, 2077–2082 (2010).
27. A. M. Enstrom, C. E. Onore, J. A. Van de Water, P. Ashwood, Differential monocyte responses to TLR ligands in children with autism spectrum disorders. *Brain Behav. Immun.* **24**, 64–71 (2010).
28. D. P. McKernan, U. Dennison, G. Gaszner, J. F. Cryan, T. G. Dinan, Enhanced peripheral toll-like receptor responses in psychosis: further evidence of a pro-inflammatory phenotype. *Transl. Psychiatry* **1**, e36 (2011).
29. P. Perez-Pardo *et al.*, Role of TLR4 in the gut-brain axis in Parkinson's disease: a translational study from men to mice. *Gut* **68**, 829–843 (2019).
30. S. Lehnardt *et al.*, Activation of innate immunity in the CNS triggers neurodegeneration through a Toll-like receptor 4-dependent pathway. *Proc. Natl. Acad. Sci. U.S.A.* **100**, 8514–8519 (2003).
31. J. J. Hu *et al.*, FDA-approved disulfiram inhibits pyroptosis by blocking gasdermin D pore formation. *Nat. Immunol.* **21**, 736–745 (2020).
32. J. K. Rathkey *et al.*, Chemical disruption of the pyroptotic pore-forming protein gasdermin D inhibits inflammatory cell death and sepsis. *Sci. Immunol.* **3** (2018).
33. J. W. Pierce *et al.*, Novel inhibitors of cytokine-induced IkappaBalpha phosphorylation and endothelial cell adhesion molecule expression show anti-inflammatory effects in vivo. *J. Biol. Chem.* **272**, 21096–21103 (1997).
34. S. Strickson *et al.*, The anti-inflammatory drug BAY 11-7082 suppresses the MyD88-dependent signaling network by targeting the ubiquitin system. *Biochem. J.* **451**, 427–437 (2013).
35. Y. Bai, S. Mei, F. Deng, J. Lieberman, X. Liu, Disulfiram blocks inflammatory TLR4 signaling by targeting MD-2. Gene Expression Omnibus (GEO). <https://www.ncbi.nlm.nih.gov/geo/query/acc.cgi?acc=GSE237028>. Deposited 11 July 2023.
36. M. L. Shen, K. L. Johnson, D. C. Mays, J. J. Lipsky, S. Naylor, Determination of in vivo adducts of disulfiram with mitochondrial aldehyde dehydrogenase. *Biochem. Pharmacol.* **61**, 537–545 (2001).
37. E. N. Petersen, The pharmacology and toxicology of disulfiram and its metabolites. *Acta Psychiatr. Scand. Suppl.* **369**, 7–13 (1992).
38. G. E. Mullen *et al.*, The role of disulfide bonds in the assembly and function of MD-2. *Proc. Natl. Acad. Sci. U.S.A.* **100**, 3919–3924 (2003).
39. M. Mancek-Keber, H. Gradisar, M. Inigo Pestana, G. Martinez de Tejada, R. Jerala, Free thiol group of MD-2 as the target for inhibition of the lipopolysaccharide-induced cell activation. *J. Biol. Chem.* **284**, 19493–19500 (2009).
40. J. E. Koo, Z. Y. Park, N. D. Kim, J. Y. Lee, Sulfuraphane inhibits the engagement of LPS with TLR4/MD2 complex by preferential binding to Cys133 in MD2. *Biochem. Biophys. Res. Commun.* **434**, 600–605 (2013).
41. C. S. Chan *et al.*, "Rejuvenation" protects neurons in mouse models of Parkinson's disease. *Nature* **447**, 1081–1086 (2007).
42. H. Park *et al.*, PAAN/MIF nuclease inhibition prevents neurodegeneration in Parkinson's disease. *Cell* **185**, 1943–1959.e1921 (2022).
43. V. Jackson-Lewis, S. Przedborski, Protocol for the MPTP mouse model of Parkinson's disease. *Nat. Protoc.* **2**, 141–151 (2007).
44. C. M. S. Silva *et al.*, Gasdermin D inhibition prevents multiple organ dysfunction during sepsis by blocking NET formation. *Blood* **138**, 2702–2713 (2021).
45. M. Zhao *et al.*, Disulfiram and diphenhydramine hydrochloride upregulate miR-30a to suppress IL-17-associated autoimmune inflammation. *J. Neurosci.* **36**, 9253–9266 (2016).
46. S. Li *et al.*, Gasdermin D in peripheral myeloid cells drives neuroinflammation in experimental autoimmune encephalomyelitis. *J. Exp. Med.* **216**, 2562–2581 (2019).
47. R. Zhou, A. S. Yazdi, P. Menu, J. Tschopp, A role for mitochondria in NLRP3 inflammasome activation. *Nature* **469**, 221–225 (2011).
48. J. Tschopp, K. Schroder, NLRP3 inflammasome activation: The convergence of multiple signalling pathways on ROS production? *Nat. Rev. Immunol.* **10**, 210–215 (2010).
49. A. P. West *et al.*, TLR signalling augments macrophage bactericidal activity through mitochondrial ROS. *Nature* **472**, 476–480 (2011).
50. G. F. Zarbato *et al.*, Dimethyl fumarate limits neuroinflammation and oxidative stress and improves cognitive impairment after polymicrobial sepsis. *Neurotox Res.* **34**, 418–430 (2018).
51. A. D. Giustina *et al.*, Dimethyl fumarate modulates oxidative stress and inflammation in organs after sepsis in rats. *Inflammation* **41**, 315–327 (2018).
52. X. Liu *et al.*, Inflammasome-activated gasdermin D causes pyroptosis by forming membrane pores. *Nature* **535**, 153–158 (2016).